

Nanoscale

Accepted Manuscript



This is an *Accepted Manuscript*, which has been through the Royal Society of Chemistry peer review process and has been accepted for publication.

Accepted Manuscripts are published online shortly after acceptance, before technical editing, formatting and proof reading. Using this free service, authors can make their results available to the community, in citable form, before we publish the edited article. We will replace this *Accepted Manuscript* with the edited and formatted *Advance Article* as soon as it is available.

You can find more information about *Accepted Manuscripts* in the [Information for Authors](#).

Please note that technical editing may introduce minor changes to the text and/or graphics, which may alter content. The journal's standard [Terms & Conditions](#) and the [Ethical guidelines](#) still apply. In no event shall the Royal Society of Chemistry be held responsible for any errors or omissions in this *Accepted Manuscript* or any consequences arising from the use of any information it contains.

Hollow Octahedral and Cuboctahedral Nanocrystals of Ternary Pt-Ni-Au Alloys

Meital Shviro[§], Shlomi Polani,[§] David Zitoun*

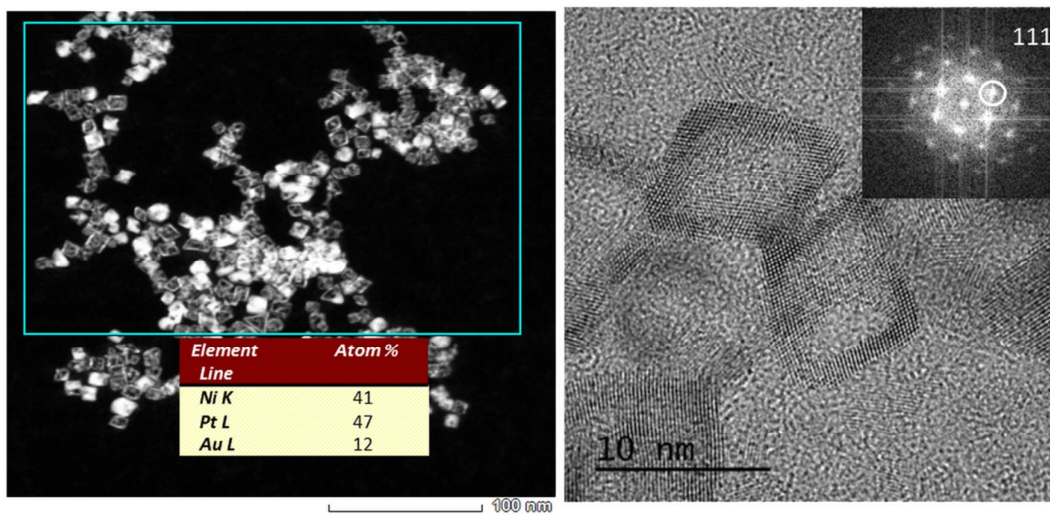
*Bar Ilan University, Department of Chemistry and Bar Ilan Institute of Nanotechnology and
Advanced Materials (BINA), Ramat Gan 52900, ISRAEL*

David.Zitoun@biu.ac.il

*Keywords: nanoparticles, hollow, galvanic replacement, superparamagnetism,
heterojunction*

Hollow particles of Pt-Ni-Au alloys have been prepared through a two-step reaction with a synthesis of NiPt octahedral and cuboctahedral templates followed by galvanic replacement reaction by Au(III). The metal etching presents an efficient method to yield hollow particle and investigate the Au diffusion in the metallic Pt-Ni framework through macroscopic (X-Ray Diffraction, SQUID magnetic measurement) and microscopic (HRTEM, STEM) measurements. The hollow particles retain the shape of the original nanocrystals. The nucleation of Au is found to be induced preferentially on the tip of the polyhedral nanocrystals while the etching of Ni starts from the facets leaving hollow octahedral particles consisting of 2 nm thick edges. In the presence of oleylamine, the Au tip grows and yields a heterogeneous dimer hollow-NiPt/Au. Without oleylamine, the Au nucleation is followed by Au diffusion in the Ni/Pt framework to yield a hollow single crystal Pt-Ni-Au alloy. The Pt-Ni-Au alloyed particles display a superparamagnetic behavior at room temperature.

[§] These authors contributed equally to the article.



1. Introduction

Hollow metallic nanoparticles have been the center of an intense scientific activity in the past years due to their potential application in plasmonics,^[1] sensing,^[2] catalysis,^[3] electrocatalysis^[4] or drug delivery.^[5] The metallic hollow nanocrystals have been mainly investigated for noble metals.^[6] The most successful synthesis routes use reactions on metallic templates by galvanic replacement,^[7] Kirkendall effect,^[8] or the spontaneous dealloying of a binary alloy.^[9]

The advances in the preparation of binary alloys Pt/Ni nanoparticles with controlled size,^[10] shape^{[11],[12]} and carbon support^[13,14] has driven a considerable interest for these nanoparticles to be used as oxygen reduction reaction (ORR) electrocatalysts in proton exchange membrane fuel cells (PEMFCs).^[15] This binary alloy Pt/Ni exhibits the highest performances reported so far but draws serious concerns on the longevity of the membrane electrode assembly (MEA) with Ni dissolution in the acidic electrolyte.^[16] Following the well-known preparation of Raney nickel, the case of Pt/Ni binary alloy has been widely investigated in the recent years;^[12,17–19] indeed, nickel can be etched selectively while platinum remains in a controlled corrosion by the oxidant. The dealloying process usually ends with the stable composition of the binary alloy. In the case of Pt/Ni, both on thin films and nanocrystals, the final composition of the alloy reaches an atomic ratio close to Pt₈₀Ni₂₀ (PtNi_{0.25}).^[20] The improvement of dealloying is needed to achieve more freedom on the final composition of the alloy and its shape. As an outstanding example of tailored shape control, a slow oxygen etching process of Pt₃₃Ni₆₆ octahedral NCs assisted by oleylamine has yielded Pt₇₅Ni₂₅ octahedral frameworks.^[21] By addition of a chelate ligand, concave Pt/Ni alloys have been obtained through coordination assisted chemical etching process.^[22] A strict limitation can be observed using a dealloying process, even modified to design a specific shape. The dealloying process ends with the stable composition of the binary alloy, according to the thermodynamics of the system.

Herein, we propose to work with a third metal to assist the etching by galvanic displacement and to study the regioselective displacement on polygonal shapes: octahedron and cuboctahedron. The addition of a third metal can circumvent some of the limitations of the previously reported etching routes by allowing different Pt/Ni ratio and by the incorporation of the third metal in a ternary alloy.^[23]

In this manuscript, we report on the etching of Pt-Ni octahedral and cuboctahedral particles by a Au(III) complex. The metal etching presents an efficient method to yield hollow particle and investigate the metal diffusion in the metallic Pt-Ni framework through macroscopic (X-Ray Diffraction, SQUID magnetic measurement) and microscopic (HRTEM, STEM) measurements.

2. Results and Discussion

2.1 Synthesis and characterization

We use a synthetic method reported by Li et al to yield Pt-Ni octahedral or cuboctahedral nanocrystals.^[11] The method has been slightly modified to yield larger batches (~ 70 mg of dry nanoparticle powder) suitable for the following galvanic displacements. The nanocrystals have been synthesized in benzyl alcohol as both solvent and reducing agent while polyvinylpyrrolidone and benzoic acid act as surfactants. The nanocrystals display an octahedral shape with regular size of 14.1 ± 1.6 nm (apex to apex) (Fig. 1A). The electron diffraction is typical of a face-centered cubic phase with a lattice parameter of 3.56 Å (close to FCC Ni: 3.524 Å).

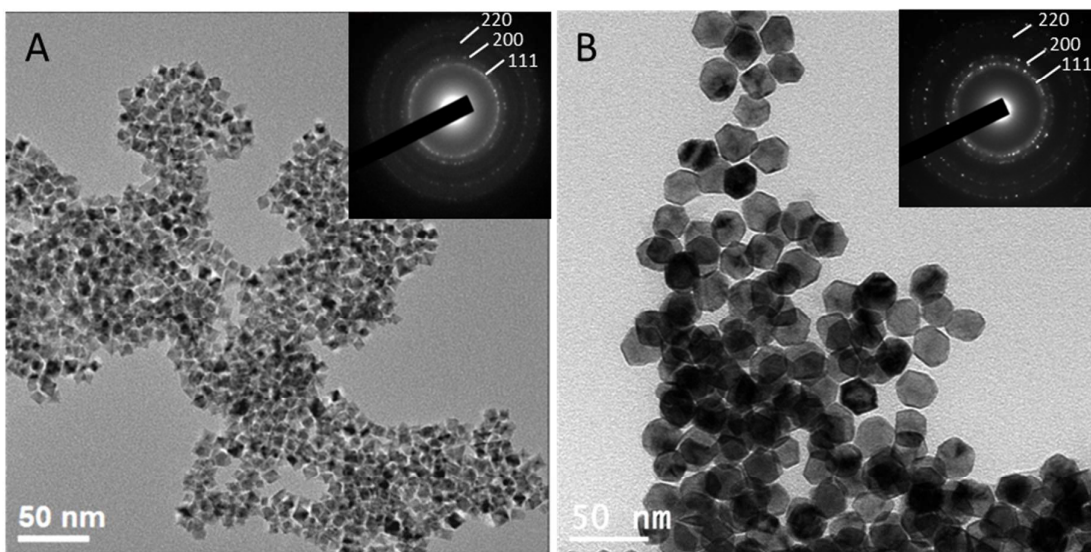
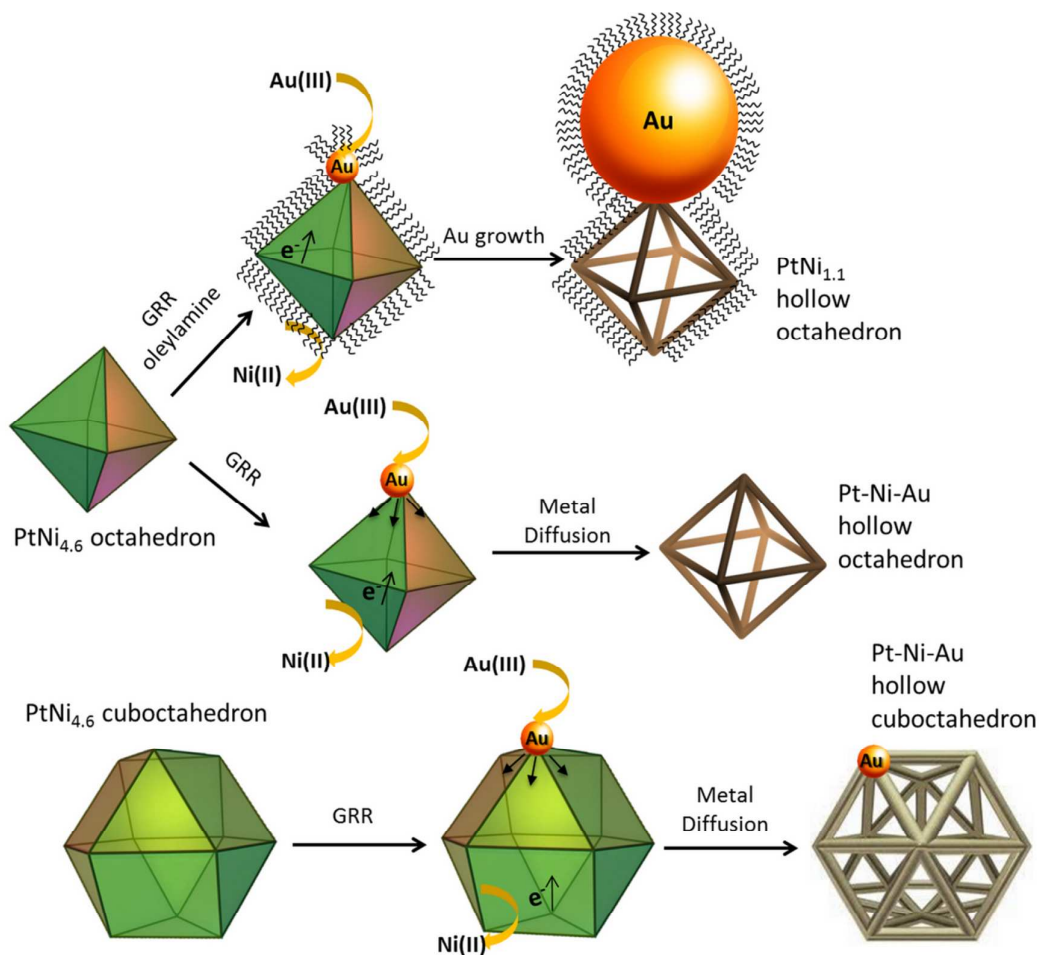


Fig. 1: Bright field transmission electron microscopy (TEM) and corresponding selective electron diffraction of PtNi_{4.8} octahedral (A) and cuboctahedral nanocrystals (B).

The octahedral nanocrystals are bounded by their {111} facets. The atomic composition Pt-Ni has been set to PtNi_{4.8} by the initial stoichiometry of metal acetylacetonate precursors, which is confirmed

by inductively coupled plasma atomic emission spectroscopy (ICP-AES) analysis and electron dispersive X-ray spectroscopy (EDS) analyses of single particle and ensembles.

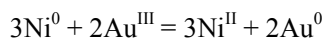
A slight change in the ligands used during the synthesis allows the stabilization of cuboctahedral particles by replacing benzoic acid with aniline.^[11] The cuboctahedra are truncated octahedra with both {111} and {100} facets as a result of aniline stabilization of the {100} facets. The cuboctahedra are homogeneous with a mean size of 21.7 ± 2.7 nm apex to apex. The nanoparticles crystallize in the same FCC phase as the octahedral particles and the stoichiometry is also set to PtNi_{4,8}.



Scheme 1: Synthetic routes to the formation of PtNi/Au dimers or Pt-Ni-Au alloys

The octahedral and cuboctahedral nanocrystals display defined shape and composition which make them suitable for an investigation of galvanic replacement reaction (GRR) by a third metal. Gold has been chosen due to its high redox potential which allows the spontaneous reaction with nickel

according to the following chemical equilibrium reaction:



Platinum itself is not corroded by Au^{III} under the synthetic conditions of temperature, pressure and concentration. The chemical equilibrium is certainly displaced to the right even though the knowledge of equilibrium constants is impeded by the use of non-aqueous solvents for the reaction. Indeed, the reaction is conducted in a mixture of toluene and ethanol with an excess of Au^{III} (Ni/ Au^{III} stoichiometry 1:2). *The GRR reaction is performed in the presence or absence of oleylamine, which appears to be a crucial component for the reaction.* The synthetic routes are reported in the schema 1.

In the presence of oleylamine ligand, $\text{PtNi}_{4.8}$ octahedra dispersion reacts with Au^{III} at room temperature overnight to yield gold nanocrystals attached to hollow Pt-Ni octahedra (Fig. 2A-D). Each Pt-Ni octahedron is attached to one Au nanocrystal through one of the apexes and, in some cases, the Au NCs coalesce to form worm-like particles, as illustrated on figure 2B. Large scale TEM images show the arrangement of Pt-Ni and Au NCs, like dimers (Fig. 2C). As reported in the general GRR mechanism, Ni(II) leaches out of the nanoparticles yielding $\text{PtNi}_{1.1}$ hollow particles. The gold assisted non-aqueous etching does not lead to the formation of $\text{PtNi}_{0.25}$ even in the presence of large excess of Au^{III} . The formation of Au NCs is obvious from the HRTEM (Fig. 2B) where an elongated Au NC joins the apexes of several PtNi hollow octahedra. Au can form very large nanostructures and EDS analysis of single nanocrystal show the high Au content ($\sim 84\%$) (Fig. 2C-D). Such a chemical composition results from a complete reaction of Au(III) to Au(0). Only Au overgrowth after the GRR process can explain this high Au atomic content.

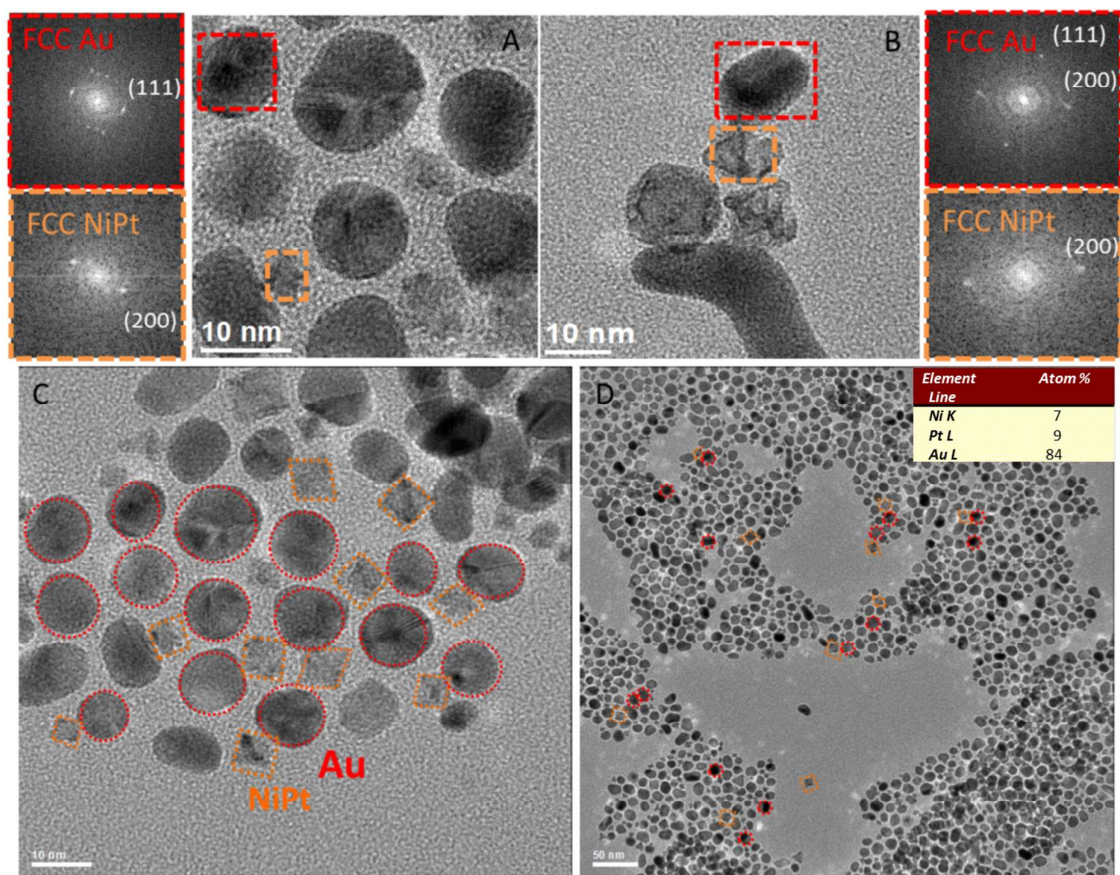


Fig 2: Bright field TEM of octahedral $\text{PtNi}_{4.8}$ nanocrystals after etching with Au(III) /oleylamine complex with selected area diffraction corresponding to Au (red square) and PtNi (orange square) (A); TEM of several hollow octahedral nanocrystals with Au particles bond to their tips and selected electron area diffraction (B); low magnification TEM and elemental composition from the electron dispersive X-ray spectroscopy (EDS) corresponding to Au (red circles) and PtNi (orange diamonds) (C-D)

The formation of Au nanocrystals attached to the $\text{PtNi}_{1.1}$ starts from the galvanic displacement on the apex of the $\text{PtNi}_{4.8}$ (schema on Fig. 2B) and the leaching of Ni^{II} is enabled by the presence of oleylamine to form a complex. Oleylamine is not limited to its role as a ligand both for Au^{III} and Ni^{II} , oleylamine is also known as a reducing agent and a ligand for metallic particles.^[24] However, a controlled experiment in the same conditions does not show any nucleation of Au particles without the presence of $\text{PtNi}_{4.8}$, which does not rule out a further role of oleylamine in the overgrowth and stabilization of Au NCs.

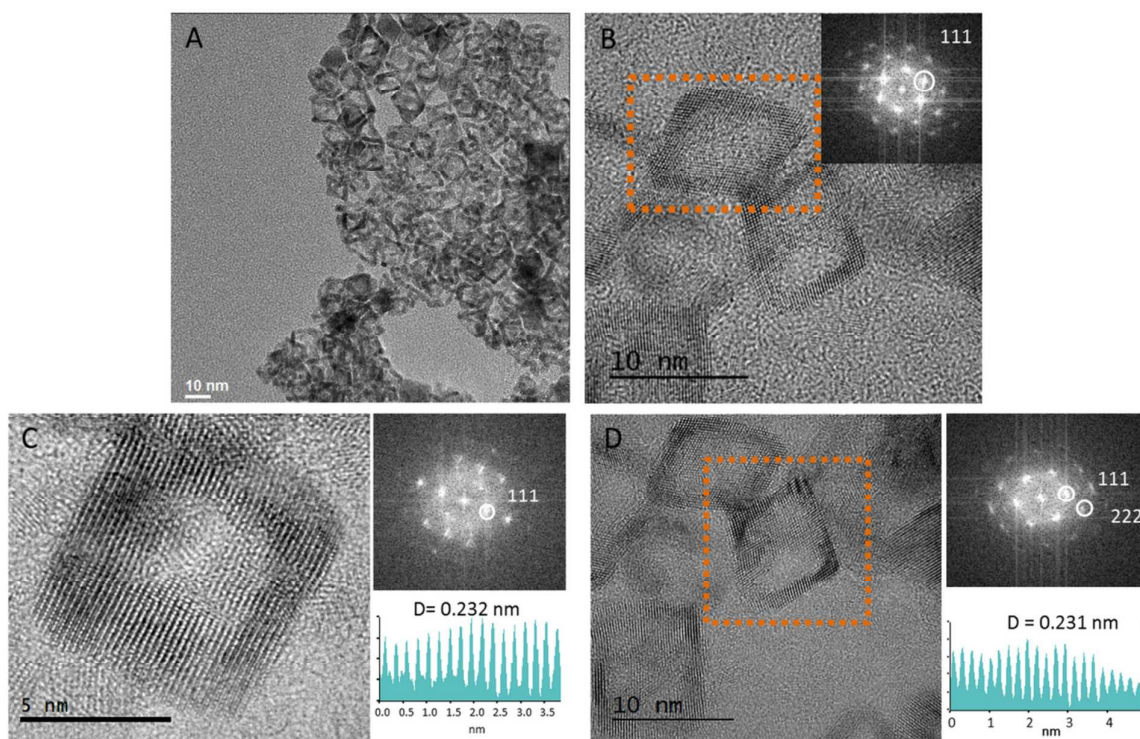


Fig. 3: Bright field TEM of octahedral $\text{PtNi}_{4.8}$ nanocrystals after etching with Au(III) (A); HRTEM of single crystalline hollow framework with the corresponding fast-Fourier transform (FFT) of the images and lattice parameter (B-D)

Therefore, we have investigated the GRR reaction *in the absence of oleylamine*. The reaction is conducted in the same conditions of temperature and concentration, still with an excess of Au^{III} ($\text{Ni}/\text{Au}^{\text{III}}$ stoichiometry 1:2) overnight. The $\text{PtNi}_{4.8}$ octahedral NCs are completely etched and show only the frame of the octahedra without visible Au NCs (Fig. 3A). These nanoframes correspond to hollow octahedra and the frame shows an architecture of edges. The edges are extremely thin (1.8 ± 0.2 nm) and highly crystalline with a FCC lattice (Fig. 3B-D). Each nanoframe is single crystalline (Fig. 3B-D). The fast-Fourier transform (FFT) of the images show the orientation of the crystal, the edges are $\{111\}$ planes for all the nanoframes. The orientation is similar to the solid octahedral particles (Fig. 1). The hollow octahedral nanoframes lie on one of the $\{111\}$ facets. The $\{111\}$ planes show an interplanar distance of 0.231 nm which corresponds to a cell parameter of 0.400 nm for a face-centered cubic (FCC) cell.

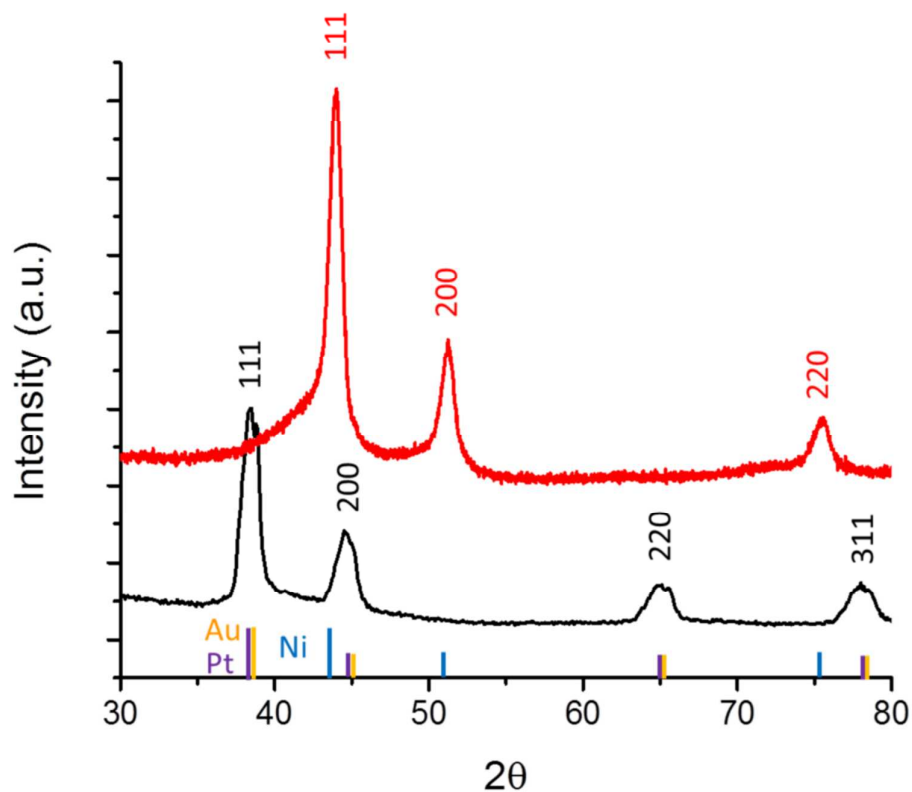


Fig. 4: Powder X-ray diffractograms of PtNi_{4.8} octahedral nanocrystals before (red) and after (black) Au(III) etching without oleylamine (standard Pt, Au and Ni main reflections added as a guideline)

On the macroscopic scale, the particles are trimetallic, according to EDS and ICP-AES measurements, with a chemical formula of PtNi_{1.1}Au_{0.8}. The powder X-ray diffraction of the samples (PtNi_{4.8} octahedra and PtNi_{1.1}Au_{0.8} hollow octahedra) reflects the changes in the lattice parameter after Au^{III} etching (Fig. 4). The pristine material can be indexed in the Fm-3m group with a lattice parameter $a = 3.550 \text{ \AA}$, very close to the lattice parameter of FCC Ni (3.524 \AA). After Au^{III} etching, the lattice parameter increases to 4.037 \AA , very close to Au (4.078 \AA). Assuming the formation of an ideal alloy of formula PtNi_{1.1}Au_{0.8}, the calculated value of the lattice parameter following a Vegard Law would be 3.86 \AA . A further analysis of the ternary alloy is limited by the absence of bulk data on this ternary alloy at room temperature.

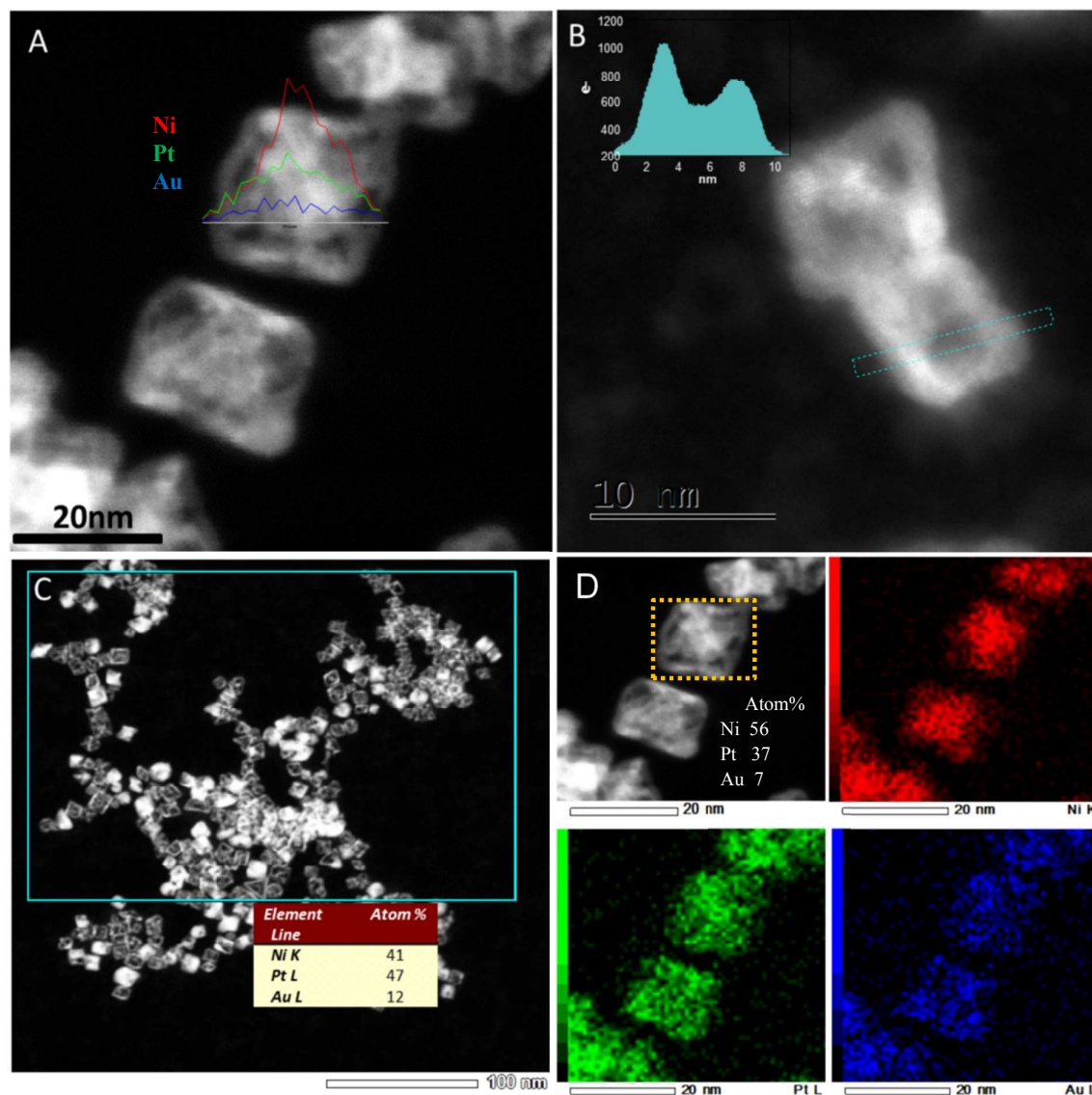


Fig. 5: High-angle annular dark-field scanning TEM (HAADF-STEM) images of octahedral $\text{PtNi}_{4.8}$ nanocrystals after etching with Au(III) at low magnification with EDS linescan (A); HAADF-STEM with electronic density profile on a single hollow octahedral nanocrystal (B); HAADF-STEM low magnification image with corresponding EDS (C); HAADF-STEM image and corresponding EDS mapping (D)

The nanoframes have been observed in dark field mode with HAADF-STEM to probe their electronic density (Fig. 5). All of the particles observed on the TEM grid display a hollow structure and the majority of them present an octahedral frame (Fig. 5C). A minority of hollow nanocrystals display

frames of cuboctahedra and trigonal pyramids. In some cases, the edges are segmented and the hollow octahedra exhibit more nanoporosity with more irregular pores and voids. Based on HAADF-STEM images of a significant collection of particles (Fig. 5C), more than 80% of the particles consist of hollow octahedra. The HAADF-STEM linescan analysis of a single octahedral nanocrystal confirms the hollow character of the octahedra with some asymmetry found from the left edge to the right edge (Fig. 5B). In fact, this inhomogeneity can be observed in most of the hollow frames which could be consistent with a discrepancy in electronic density within a particle arising from a gradient of atomic composition. Within a single octahedral nanocrystal, the composition has been checked by EDS linescan (Fig. 5A) and by EDS mapping (Fig. 5D), both measurements are consistent with an homogeneous composition. The octahedral nanocrystals are single-crystalline statistical alloys within the resolution of the EDS (~ 1 nm).

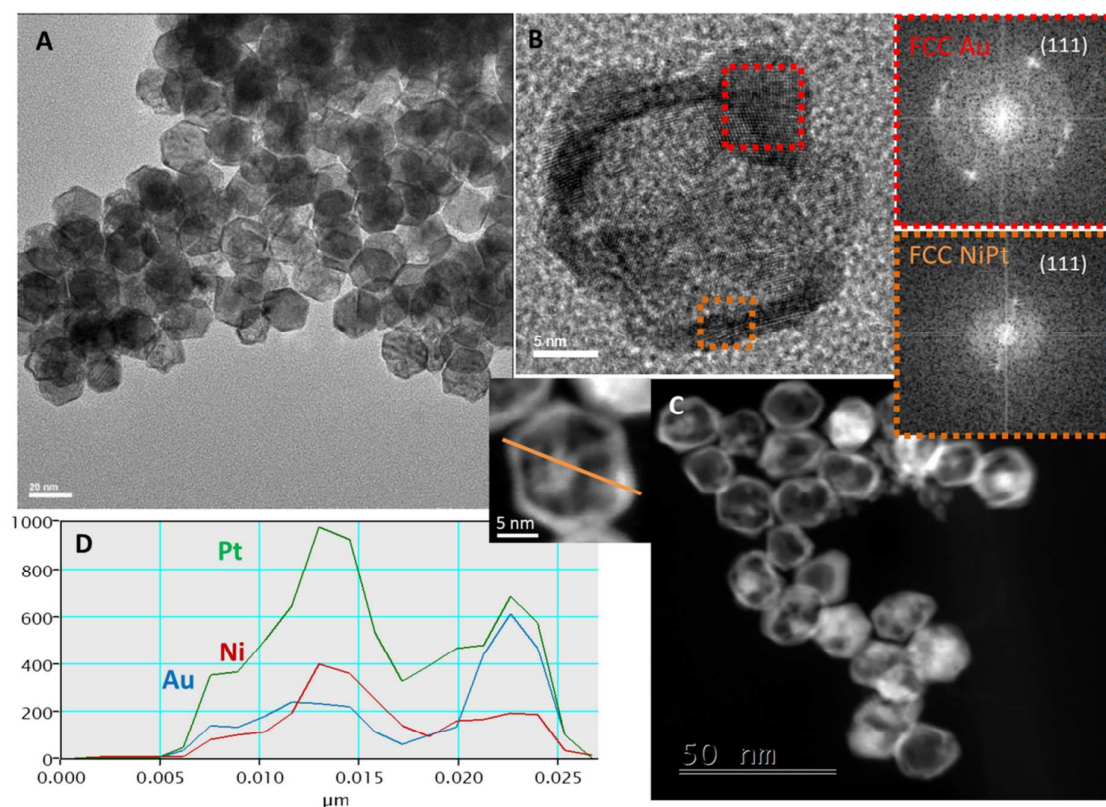


Fig. 6: Bright field TEM of cuboctahedral PtNi_{4.8} nanocrystals after etching with Au(III) (A); HRTEM of a single particle with FFT (B); HAADF-STEM of low magnification image (C); HAADF-STEM of a single particle with elemental profile along the orange line from EDS (D)

The same reaction has been carried out on cuboctahedral PtNi_{4.8} NCs. The surfactant-free etching process in Au(III) solution yields hollow cuboctahedral particles (Fig. 6A). The cuboctahedral shape is easily noticeable from TEM images with particles displaying the same size as the solid cuboctahedral particles observed on Fig.1B. The wall thickness deduced from HRTEM is also very thin (2 ± 0.4 nm) with a rough surface compared with the very smooth hollow octahedra (Fig. 6B). The observed porosity displays a more disordered structure. As pointed above, the GRR process occurs preferentially on the tips of the solid polyhedral particles to yield hollow cubocthedra (Fig. 6C).

Indeed, the hollow nanocrystals display some inhomogeneities in the atomic ratios of Ni, Pt and Au. HAADF –STEM line scan has been combined with HAADF-STEM-EDS line scan to provide both the electronic density and elemental composition on single hollow cuboctahedral nanocrystals (Fig. 6D). The electronic density profile confirms the void between walls of 2-3 nm thickness. The EDS line scan shows typically a similar profile for Ni, Pt and Au except on one specific region of the particle. On Fig.6B, this region, located on the right tip of the hollow polyhedron, shows a high Au content and a lower Ni content. This observation is typical for all the hollow cuboctahedra observed and can be interpreted as the Au nucleation site during the GRR process.

2.2. Magnetic properties

The magnetic properties of Ni-Pt-Au alloys are not reported in the literature, neither for bulk or nanoscale samples, which makes our study an important landmark. Noteworthy, magnetic properties are highly sensitive to the percentage of ferromagnetic Ni in the alloys and to the surface states of the nanocrystals. The magnetic measurements could then be used to follow the GRR process and assess the surface states of the nanocrystals. The magnetic properties of octahedral PtNi_{4.8} NCs and octahedral hollow PtNi_{1.1}Au_{0.8} (without oleylamine) have been checked in a superconducting quantum interference device (SQUID). The magnetic field dependence of the magnetization has been collected at low temperature ($T = 2$ K) to get closer to the saturation magnetism (Fig. 7A). At 2 K, PtNi_{4.8} octahedral NCs shows an average magnetic moment of $\sigma = 0.41 \mu_B/\text{atom}$ at 5 T which can be

compared with the value of $\sigma = 0.48 \mu_B/\text{atom}$ for the bulk $\text{PtNi}_{4.8}$ alloy. These values are close enough to further evidence the metallic character of the particles and the absence of a dead layer arising from strongly interacting surface ligands^[25] but, actually, could also be consistent with a concentration gradient of Pt and Ni within the particle, since the calculated magnetization for a biphasic Pt-Ni particle ($\sigma = 0.49 \mu_B/\text{atom}$) would also match the experimental value.^[26] The Curie temperature of the bulk PtNi alloy shows also a linear decrease with Pt although the experimental temperature dependence of the magnetism for the $\text{PtNi}_{4.8}$ octahedral NCs is dominated by the superparamagnetic regime observed above the blocking temperature of $T_B = 70 \text{ K}$ (Fig. 7B).

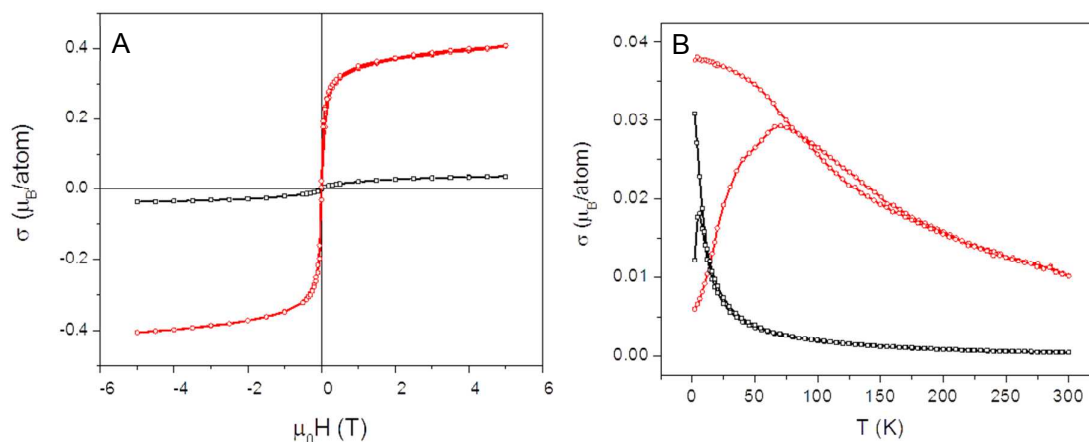


Fig. 7: Hysteresis loop of the magnetization per metal atom at $T = 2\text{K}$ for $\text{PtNi}_{4.8}$ (red circles), $\text{PtNi}_{1.1}\text{Au}_{0.8}$ (black squares) (A) and temperature dependence of the magnetization per metal atom at $\mu_0 H = 0.005 \text{ T}$ (B)

Since the nanocrystals display a superparamagnetic behavior above 70 K , the measurement of Curie temperature ($T_C = 450 \text{ K}$, bulk value)^[27] remains out of range.

After the GRR step, the hollow octahedral $\text{PtNi}_{1.1}\text{Au}_{0.8}$ NCs display much lower values of magnetization ($\sigma = 0.037 \mu_B/\text{atom}$) and blocking temperature ($T_B = 6 \text{ K}$). Such a drastic decrease results from the dilution of Ni atoms with Pt and Au diamagnetic atoms and is consistent with the elemental mapping. The bulk magnetic values being unavailable, we have compared our experimental values to the Pt_2Ni alloy with identical Ni atomic fraction. The magnetic phase diagram shows the transition from ferromagnetism to paramagnetism for this exact composition which explains the

almost vanishing magnetic moment^[27] and the low blocking temperature. In fact, the maximum in the zero-field-cooled could also be interpreted as the Curie temperature for the system. The very sharp transition clearly emphasizes the homogeneity of the hollow particles, both in size and composition. This macroscopic measurement confirms the results of electron microscopy with two main outcomes: i) all the NCs have been etched; ii) the Ni atoms are alloyed with diamagnetic metals. Moreover, the high magnetic moment found for the two samples (comparable to bulk values) shows that, even for extremely small features, like the nanoframes, the ligands used for stabilization do not affect the surface magnetism.

2.3 Discussions

The galvanic replacement reaction (GRR) by Au(III) has been successfully applied to PtNi_{4.8} solid polyhedral nanocrystals, either on octahedral or cuboctahedral templates. The reaction involves two steps of Ni etching and Au deposition which result in the PtNi_{1.1}Au_{0.8} hollow particles with the same shape as the template. X-Ray diffraction and selected area electron diffraction reveals the formation of a crystalline phase with lattice parameters close to FCC Au. Magnetic measurements points out at the dilution of Ni atoms in the ternary phase during the etching/alloying process with a transition from a high magnetic moment superparamagnetic PtNi_{4.8} alloy to a paramagnetic PtNi_{1.1}Au_{0.8} ternary alloy.

The octahedral hollow particles show well-defined 2 nm thick single crystalline edges while the cuboctahedral hollow particles display a rough surface. In all cases, the reaction begins with a nucleation of Au on the surface of the particle (tip for the octahedral, tip or edge for the cuboctahedral shape), with concomitant Ni etching. The Au tip can be stabilized and experienced overgrowth in the presence of oleylamine whereas it diffuses within the framework of the edges without oleylamine. Even in the latter case, the fingerprint of Au nucleation site has been observed by HAADF-STEM-EDS measurements on a tip of the hollow cuboctahedra. Oleylamine is well known for its versatile use as both ligand (in the Au(III) complex), transfer agent for GRR in biphasic medium,^[28] surfactant for the colloids^[24] and reducing agent to promote the noble metal overgrowth.^[29] The influence of the reducing agent concentration has also been reported in the case of Pd-Pt hollow alloyed nanocrystals which demonstrate the competition between galvanic replacement and reducing agent assisted

deposition of Pt on Pd.^[30]

As pointed in the introduction, the scientific literature provides very nice examples of etching Pt-Ni alloys towards Pt rich hollow nanocrystals. In the following, we shall discuss the analogies between the etching/alloying ternary system Pt/Ni/Au investigated herein and the etching Pt/Ni binary system reported before. As demonstrated on acidic etching of PtNi₃ bimetallic particles without a defined shape, the etching of Ni can be assisted by dissolved O₂ to yield porous particles while the same process in N₂ yields solid particles with Pt enriched skin.^[31] The acidic etching of shape controlled PtNi₃ or PtNi₂ NCs seems too aggressive to conserve the initial shape of the nanoparticles^[20] and chelate ligands have been used as etching agents to yield concave octahedral NCs.^[22]

In a striking example, the mild O₂ etching schema has been applied to well-defined octahedral PtNi₃ nanocrystals based on free corrosion in air.^[21] The resulting Pt₃Ni octahedral nanoframes show a higher Pt content on the tips of the octahedra. This Pt enriched regions could be present from the synthesis itself before any etching process, as demonstrated by the Pt-rich frame/Ni rich facets observed for Pt_{1.5}Ni, PtNi and PtNi_{1.5} octahedral NCs.^[32]

The etching of Ni towards Ni(II) molecular species occurs preferentially at Ni-rich regions and such a segregation of Ni on the {111} facet regions could explain the synthesis of noble metal rich nanoframes.^[21,32] The reaction of Au(III) on NiPt_{4.8} polyhedral particles brings more information to unravel the regio-selectivity of the etching mechanism. The gold nucleation site can be followed by electron microscopy imaging in the presence of oleylamine which provides an overgrowth of the gold colloid. The nucleation occurs on one specific apex, as already observed for the formation of heterogeneous nanostructures, albeit not hollow.^{[33][34]} On octahedral NCs, the nucleation occurs on the tip while the etching of Ni goes through the facets, with a concomitant diffusion of Au through the edges in the absence of oleylamine. On cuboctahedral particles, the discrepancy in terms of reactivity towards Au(III) between the tip/edges and the (200) facets does not seem high enough to observe a preferential deposition of Au on the tip/edges only, contrary to the schematic view reported on a related Pt-Ni-Au system.^[23]

3. Conclusion

Hollow particles of Pt/Ni/Au alloys have been prepared through a two-step reaction with a synthesis of NiPt octahedral and cuboctahedral templates followed by galvanic replacement reaction by Au(III). The hollow particles retain the shape of the original nanocrystals. The nucleation of Au is found to be induced preferentially on the tip of the octahedral nanocrystals while the etching of Ni occurs from the facets leaving a hollow octahedral particles consisting of 2 nm thick edges. The Au nucleation is followed by its diffusion in the Ni/Pt framework to yield a ternary alloy. The addition of oleylamine promotes the overgrowth of Au. The octahedral frameworks display an atomic content of 38% Ni, as demonstrated by elemental analysis and confirmed by the paramagnetic nature of the alloy. The high content of Ni has not been achieved before by chemical etching to yield hollow octahedral particle. The synthesis reported here paves the way to the formation of hollow polyhedral nanocrystals consisting in ternary alloys.

4. Experimental Section

Materials:

Benzylalcohol (99%, pure), oleylamine (80-90%) and aniline (99.5%) were acquired from ACROS, benzoic acid (ACS, 99.5%), H₂AuCl₄ (49.5% Au) and poly(vinylpyrrolidone) (PVP), (MW = 8000, AR) were purchased from Alfa Aesar, Platinum (II) acetylacetonate (Pt(acac)₂) (98%, Strem), Nickel (II) acetylacetonate (Ni(acac)₂), (95%, Sigma Aldrich). All of the chemicals above were used without further purification.

Synthesis of Pt/Ni Nanocrystals. In a typical synthesis of PtNi_{4.8} octahedral nanocrystals, Pt(acac)₂, (0.2 mmol), poly(vinylpyrrolidone) (PVP, MW = 8000), (0.08 g) Ni(acac)₂ (0.93 mmol) and benzoic acid (4.0 mmol) were dissolved in 50 mL of benzyl alcohol by 30 min of vigorous stirring. The resulting homogeneous green solution was transferred into a 100 mL Ace pressure glass flask. The sealed vessel was then heated to 150 °C for 12 h before it was cooled down to room temperature. The products were precipitated by acetone, separated via centrifugation, and further purified by an ethanol– acetone mixture. The truncated octahedral nanocrystals were synthesized followed the above procedure by replacing the benzoic acid with aniline (5 mL).

Etching of NiPt Nanocrystals. PtNi_{4.8} nanocrystals are synthesized by the procedure described

above. The solution of Au(III) is prepared by dissolving 0.025 mmol HAuCl_4 either in 2 mL oleylamine (referred in the manuscript as the synthesis with oleylamine) or in 2 mL toluene and 100 μL ethanol (referred as without oleylamine). The yellow solutions are added dropwise to the $\text{PtNi}_{4.8}$ nanocrystals black dispersion in ethanol (10 mg in 2 mL) under vigorous mixing. The atomic ratio of Au/Ni is set to 2:1. The dark dispersion is stirred overnight at room temperature and turns purple in the presence of oleylamine. Ethanol and toluene are then added, and the dispersion is centrifuged three times at 4000 rpm for 8 min to separate the solid product.

Characterization: TEM, XRD, SQUID

The structure of the NPs is investigated by transmission electron microscopes (TEM): JEOL 1400 at 120 kV, JEOL JEM-2100 (LaB6) at 200 kV and Hitachi HF3300 for high resolution imaging (HRTEM). Fourier transform analysis (FFT) of high-resolution images technique was used for structural analysis. HRTEM with energy dispersive X-ray spectroscopy (EDS) were obtained on a JEOL JEM-2100F Field Emission Electron Microscope operated at 200 kV.

X-Ray Diffractograms are collected on a Rigaku Smartlab X-Ray Diffractometer. The nanocrystals are drop-cast on a glass slide.

Magnetic properties are measured using a Superconducting Quantum Interference Design (SQUID) magnetometer MPMS XL7, in the range of temperature 2–300 K and of field 0–5 T. The temperature-dependent susceptibility was measured using DC procedure. The samples are cooled to 2K under zero magnetic field, low magnetic field (5.0 mT) was applied and data collected from 2 K to 300 K (zero-field cooled, ZFC). Field Cooled (FC) measurements were performed from 2 K to 300 K with an applied field during the cooling. Hysteresis loop was measured at 2 K.

ACKNOWLEDGMENTS:

The authors warmly thank Dr Etienne Snoeck (CEMES, CNRS, France) and Dr Vladimir Ezersky (Ben Gurion University, Israel) for their assistance with HRTEM. This work was supported by the I-

CORE program of the planning and budgeting committee and the Israel Science Foundation (2797/11).

- [1] M. J. Mulvihill, X. Y. Ling, J. Henzie, P. Yang, *J. Am. Chem. Soc.* **2010**, 895.
- [2] J. Biener, A. Wittstock, L. A. Zepeda-Ruiz, M. M. Biener, V. Zielasek, D. Kramer, R. N. Viswanath, J. Weissmüller, M. Bäumer, A. V. Hamza, *Nat. Mater.* **2009**, 8, 47.
- [3] B. Wu, N. Zheng, *Nano Today* **2013**, 8, 168.
- [4] Y. Xu, B. Zhang, *Chem. Soc. Rev.* **2014**, 43, 2439.
- [5] K. An, T. Hyeon, *Nano Today* **2009**, 4, 359.
- [6] Y. Sun, B. Mayers, Y. Xia, *Adv. Mater.* **2003**, 15, 641.
- [7] C. M. Cobley, Y. Xia, *Mater. Sci. Eng., R* **2010**, 70, 44.
- [8] W. Wang, M. Dahl, Y. Yin, *Chem. Mater.* **2013**, 25, 1179.
- [9] J. Erlebacher, M. J. Aziz, A. Karma, N. Dimitrov, K. Sieradzki, *Nature* **2001**, 410, 450.
- [10] Y. Yu, W. Yang, X. Sun, W. Zhu, X.-Z. Li, D. J. Sellmyer, S. Sun, *Nano Lett.* **2014**, 1.
- [11] Y. Wu, S. Cai, D. Wang, W. He, Y. Li, *J. Am. Chem. Soc.* **2012**, 134, 8975.
- [12] J. Zhang, H. Yang, J. Fang, S. Zou, *Nano Lett.* **2010**, 10, 638.
- [13] C. Cui, L. Gan, M. Neumann, M. Heggen, B. R. Cuenya, P. Strasser, *J. Am. Chem. Soc.* **2014**, 136, 4813.
- [14] C. Zhang, S. Y. Hwang, A. Trout, Z. Peng, *J. Am. Chem. Soc.* **2014**, 136, 7805.
- [15] X. Zhou, Y. Gan, J. Du, D. Tian, R. Zhang, C. Yang, Z. Dai, *J. Power Sources* **2013**, 232, 310.
- [16] X. Tuaeov, S. Rudi, V. Petkov, A. Hoell, P. Strasser, *ACS Nano* **2013**, 7, 5666.
- [17] S. I. Choi, S. Xie, M. Shao, J. H. Odell, N. Lu, H.-C. Peng, L. Protsailo, S. Guerrero, J. Park, X. Xia, J. Wang, M. J. Kim, Y. Xia, *Nano Lett.* **2013**, 13, 3420.
- [18] C. Zhang, S. Y. Hwang, A. Trout, Z. Peng, *J. Am. Chem. Soc.* **2014**, 136, 7805.
- [19] W. Yu, M. D. Porosoff, J. G. Chen, *Chem. Rev.* **2012**, 112, 5780.
- [20] D. Wang, P. Zhao, Y. Li, *Sci. Rep.* **2011**, 1, 37.
- [21] C. Chen, Y. Kang, Z. Huo, Z. Zhu, W. Huang, H. L. Xin, J. D. Snyder, D. Li, J. a Herron, M. Mavrikakis, M. Chi, K. L. More, Y. Li, N. M. Markovic, G.A. Somorjai, P. Yang, V. R. Stamenkovic, *Science* **2014**, 343, 1339.
- [22] Y. Wu, D. Wang, Z. Niu, P. Chen, G. Zhou, Y. Li, *Angew. Chem. Inter. Ed.* **2012**, 51, 12524.
- [23] Y. Wu, D. Wang, G. Zhou, R. Yu, C. Chen, Y. Li, *J. Am. Chem. Soc.* **2014**, 136, 11594.

- [24] S. Mourdikoudis, L. M. Liz-Marzan, *Chem. Mater.* **2013**, *25*, 1465.
- [25] N. Cordente, C. Amiens, B. Chaudret, M. Respaud, F. Senocq, M.-J. Casanove, *J. Appl. Phys.* **2003**, *94*, 6358.
- [26] D. Paudyal, T. Saha-Dasgupta, A. Mookerjee, *J. Phys. Condens. Matter* **2004**, *16*, 2317.
- [27] M. C. Cadeville, C. E. Dahmani, F. Kern, *J. Magn. Magn. Mater.* **1986**, *57*, 1055.
- [28] Y. Wang, Y. Chen, C. Nan, L. Li, D. Wang, Q. Peng, Y. Li, *Nano Res.* **2014**, *8*, 140.
- [29] M. Shviro, D. Zitoun, *J. Phys. Chem. C* **2014**, *118*, 10455.
- [30] J. W. Hong, S. W. Kang, B.-S. Choi, D. Kim, S. B. Lee, and S. W. Han, *ACS Nano*, 2012, **6**, 2410.
- [31] L. Gan, M. Heggen, R. O'Malley, B. Theobald, P. Strasser, *Nano lett.* **2013**, *13*, 1131.
- [32] C. Cui, L. Gan, M. Heggen, S. Rudi, P. Strasser, *Nat. Mater.* **2013**, *12*, 765.
- [33] T. Mokari, E. Rothenberg, I. Popov, R. Costi, U. Banin, *Science* **2004**, *139*, 1787.
- [34] J. Wu, Y. Hou, S. Gao, *Nano Res.* **2011**, *4*, 836.